Virions and respiratory droplets in air: Diffusion, drift, and contact with the epithelium

BioSystems 198 (2020) 104241

Contents lists available at ScienceDirect

BioSystems

journal homepage: www.elsevier.com/locate/biosystems

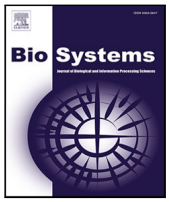

Review article

Virions and respiratory droplets in air: Diffusion, drift, and contact with the epithelium

Vladimir P. Zhdanov [a,b,*], Bengt Kasemo [a]

[a] Sections of Nano and Biological Physics and Chemical Physics, Department of Physics, Chalmers University of Technology, Göteborg, Sweden
[b] Boreskov Institute of Catalysis, Russian Academy of Sciences, Novosibirsk, Russia

ARTICLE INFO

Keywords:
Viruses
Epithelium
Respiratory droplets
Diffusion and drift
Convection
Evaporation

ABSTRACT

Some infections, including e.g. influenza and currently active COVID 19, may be transmitted via air during sneezing, coughing, and talking. This pathway occurs via diffusion and gravity-induced drift of single virions and respiratory droplets consisting primarily of water, including small fraction of nonvolatile matter, and containing virions. These processes are accompanied by water evaporation resulting in reduction of the droplet size. The manifold of information concerning these steps is presented in textbooks and articles not related to virology and the focus is there frequently on biologically irrelevant conditions and/or droplet sizes. In this brief review, we systematically describe the behavior of virions and virion-carrying droplets in air with emphasis on various regimes of diffusion, drift, and evaporation, and estimate the rates of all these steps under virologically relevant conditions. In addition, we discuss the kinetic aspects of the first steps of infection after attachment of virions or virion-carrying droplets to the epithelium, i.e., virion diffusion in the mucus and periciliary layers, penetration into the cells, and the early stage of replication. The presentation is oriented to virologists who are interested in the corresponding physics and to physicists who are interested in application of the physics to virology.

1. Introduction

Viral infections are inordinately diverse and complex, because their initiation and spread occur at very different time and length scales and include the interplay of very different processes in different strata of human population and different organs inside an each infected person. At the system level, this interplay can be clarified by using theoretical models of four complementary categories with emphasis, respectively, on (i) human populations [see, e.g., the articles by Gao et al., 2019, Fabricius and Maltz, 2020, and references therein; concerning COVID 19, see, e.g., recent studies by Bertozzi et al., 2020, De-Leon and Pederiva, 2020, and Tkachenko et al., 2020], (ii) populations of virions and cells inside an infected person [reviewed by Bocharov et al., 2018, Goyal et al., 2019, and Handel et al., 2020], (iii) interplay of intracellular kinetic steps [reviewed by Yin and Redovich, 2018 and Zhdanov, 2018], and (iv) mechanistic details of single steps of virion function including, e.g., the ways of transmission, details entry into a host cell, specifics of genome replication, and capsid formation [reviewed by Jefferys and Sansom, 2019 and Altan-Bonnet et al., 2020]. The models belonging to different categories are complementary and can be combined [see, e.g., Haseltine et al. (2005) for combining (ii) and (iii)].

Concerning the ways of transmission of virions [reviewed by Sanjuán, 2017, 2018 and Leeks et al., 2019], one can notice that the conventional scenario includes independent transport of single virions each of which contains one genome. The transmission of some of the viruses may, however, occur collectively so that multiple virions are contained inside a larger structure. One of the examples of this transmission mode includes virions aggregating either through direct contacts [as e.g. in the case of stomatitis virus (Andreu-Moreno and Sanjuán, 2020)] or through mediation by a vector such as a bacterial cell [as e.g with intestinal bacteria promoting infection of cells by poliovirus (Erickson et al., 2018)]. Another example includes transport of multiple virions by ~ 100-nm-sized extra-cellular vesicles (exosomes) as e.g. with Hepatitis A virus (Altan-Bonnet, 2016). Each vesicle may contain up to 10–20 virions (Bou et al., 2019).

In this brief theoretical review belonging to category (iv), we focus on virion transmission via air during sneezing, coughing, and talking. This pathway is operative in various infections including influenza and COVID 19 (Wölfel et al., 2020). It is realized via diffusion and gravity-induced drift of single virions or predominantly via respiratory droplets containing virions. Biologically/chemically, these droplets are formed of saliva produced and secreted by salivary glands and containing, just

* Corresponding author at: Boreskov Institute of Catalysis, Russian Academy of Sciences, Novosibirsk, Russia.
E-mail address: zhdanov@chalmers.se (V.P. Zhdanov).

https://doi.org/10.1016/j.biosystems.2020.104241
Received 12 July 2020; Received in revised form 2 September 2020; Accepted 2 September 2020
Available online 5 September 2020

after secretion, primarily water (≃99%) in combination with nonvolatile matter (≃1%) including sodium, potassium, calcium, magnesium, bicarbonate, phosphates, immunoglobulins, proteins, enzymes, mucins, and nitrogenous products, such as urea and ammonia [Humphrey and Williamson, 2001; Sarkar et al., 2019; the composition depends on age (Xu et al., 2019)]. The fraction of nonvolatile matter in droplets carrying virions can be higher [up to ≃5% (Stadnytskyi et al., 2020)]. Migration of droplets in air can be accompanied by water evaporation resulting in reduction of the droplet size. The rates of these processes depend on the shape and size of virions and size of respiratory droplets. Although often spherical, viruses can be bullet-shaped, brick-shaped, amorphous, or filamentous ranging in size from ≃20 up to ≃2000 nm (Cossart and Helenius, 2014). The diameter of spherically shaped virions (this case is under consideration herein) is often in the range from ≃20 to 250–400 nm (with maximum of 500 nm). For example, spherical lipid-membrane-enveloped influenza and (currently active) COVID 19 viruses are ≃100 nm in diameter (Li et al., 2011; Zhu et al., 2020). The size of spherically shaped droplets carrying such viruses is frequently about 0.1-20 μm or larger, up to about 100 μm during sneezing (Xie et al., 2007; Morawska et al., 2009; Zhang et al., 2015; Huang et al., 2020). Small virion-carrying droplets are expected to contain one or two virions (Stadnytskyi et al., 2020). Large droplets can contain many virions, up to about 200 (Vejerano and Marr, 2018). After contacts of such droplets with the epithelium, the corresponding cells can get one, a few, or many virions, i.e., the virions can act collectively. Thus, this mode of the transmission is an additional example of collective action (cf. the paragraph above).

Physically, virions can be viewed just as nanoparticles of one of the types, whereas respiratory droplets represent just one of the types of liquid droplets. The experimental and theoretical literature concerning diffusion and drift of nanoparticles and liquid droplets of various sizes and evaporation from such droplets is extensive and often not directly related to virology. Some of the suitable references are given below. Here, for example, we mention safety/risk-related studies focused on nanoparticles or microparticles from traffic (e.g., diesel soot), wear particles from tires, and particles in fume during covering the roads by asphalt (Marijnissen and Gradoń, 2010). Our experience indicates that despite the abundance of the literature a systematic simultaneous treatment of all these processes with the virology-relevant sizes of particles and conditions is lacking. Many of these processes are mentioned in the virology-oriented reviews (see, e.g., Gralton et al., 2011), but the articles of the latter category usually do not contain equations and do not allow one to easily understand general trends. Our goal is to fill these gaps. Bearing this goal in mind, we use the simplest well-established models and equations with minimal number of references in order to avoid numerous inferior details and to make the presentation suitable for general readership. The scale of the effects and general trends are illustrated by the corresponding original figures.

2. Diffusion, ballistic motion, and drift in stagnant air

This section is focused on diffusion (Section 2.1), ballistic motion (Section 2.2), and gravity-induced drift (Section 2.3) of single virions and respiratory droplets in stagnant air. The behavior of droplets in air strongly depends on evaporation of water. The latter process is nevertheless neglected here as well as in Section 3, because the evaporation-free cases serve as valuable reference cases and also are applicable to non-evaporative nano- or microparticles. The role of evaporation is discussed in Section 4.

2.1. Diffusion in the horizontal direction

Diffusion of single particles in stagnant air is phenomenologically described by using the conventional Fick first law containing the diffusion coefficient. The value of this coefficient and its dependence on the air properties can be calculated by using various models. If the mean free path of molecules of air (∼ 100 nm) is comparable to or larger than the particle size, the diffusion can be treated at the level of binary collisions of molecules with a particle, and the diffusion coefficient can be represented as (Lifshitz and Pitaevskii, 1981)

$$D_\circ = \frac{3(k_B T)^{3/2}}{2^{3/2}\pi^{1/2} m^{1/2} P R^2}, \tag{1}$$

where R is the particle radius, m is the average mass of molecules (it can be identified with the mass of N_2 molecules), k_B is the Boltzmann constant, T is absolute temperature, and P is pressure. In the opposite limit, the diffusion coefficient can be calculated at the level of fluid dynamics (Landau and Lifshitz, 1987)

$$D_* = \frac{k_B T}{6\pi\eta R}, \tag{2}$$

where η is the air viscosity [1.8×10^{-4} g/(s cm) at room temperature]. At arbitrary R, the diffusion coefficient can be represented as

$$D = \max(D_\circ, D_*). \tag{3}$$

A slightly more accurate fitting of the transition from (1) to (2) is given e.g. by the Cunningham expression (Moskal et al., 2010), but it contains empirical parameters. For our present goals, Eqs. (1)–(3) are sufficient.

The mean squared displacement for 2D diffusion in the horizontal direction (perpendicular to the gravitation field; x and y are the corresponding coordinates) and the average diffusion length depend on time as

$$\langle \Delta x^2\rangle + \langle \Delta y^2\rangle = 4Dt, \tag{4}$$

$$l_d = (\langle \Delta x^2\rangle + \langle \Delta y^2\rangle)^{1/2} = (4Dt)^{1/2}. \tag{5}$$

Concerning the temperature, T, in Eqs. (1) and (2) or other equations presented below, one can wonder whether it can be identified with the body or environment temperature or should be calculated as a function of time. Strictly speaking, this temperature is a function of time. The time scale characterizing the heat exchange between air and droplets is, however, rather short compared to the time scales of other processes such as transport and evaporation (see, e.g., Dbouk and Drikakis, 2020a). For this reason, T can usually be identified with the environment temperature.

Typical values of the diffusion coefficient and average diffusion shift calculated for virions and respiratory droplets by using Eqs. (1)–(5) with T = 300 K are shown in Figs. 1 and 2, respectively. On the time scale of 10 min, the shift is seen to be fairly short (about 1 cm for virions and only about 0.05 cm for droplets). Practically, this means that the virion and droplet motion in the horizontal direction usually occurs due to air convection (Section 3) rather than via conventional diffusion.

2.2. Ballistic motion in the horizontal direction

Bearing sneezing in mind, it is instructive to describe ballistic motion of a single particle in the horizontal direction (perpendicular to the gravitation field). Such motion is terminated by the friction force generated due to the interaction of a particle with the gas-phase molecules. The value of this friction force is the same as that of the external force needed to keep the particle velocity, v, constant. By definition, the velocity and the latter force are related as $v = \alpha F$, where α is the particle mobility. Thus, the friction force related to the ballistic motion of a particle in the horizontal direction is given by

$$F_h = v/\alpha. \tag{6}$$

With this friction force and in the absence of the external force, the equation for the particle velocity is as follows

$$m\,dv/dt = -v/\alpha, \quad \text{or} \quad v = v(0)\exp(-t/\alpha m), \tag{7}$$

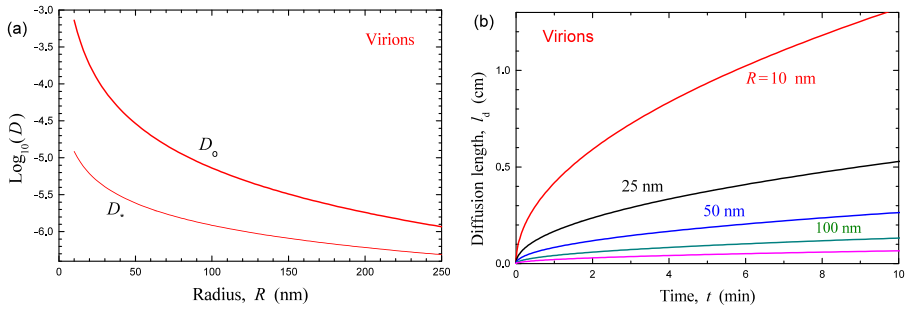

Fig. 1. (a) Coefficients of virion diffusion corresponding to binary collisions [Eq. (1)] and fluid dynamics [Eq. (2)] as a function of the virion radius and (b) average diffusion length [Eq. (5)] as a function of time for $R = 10$, 25, 50, 100, and 200 nm. In this case, binary collisions [Eq. (1)] dominate.

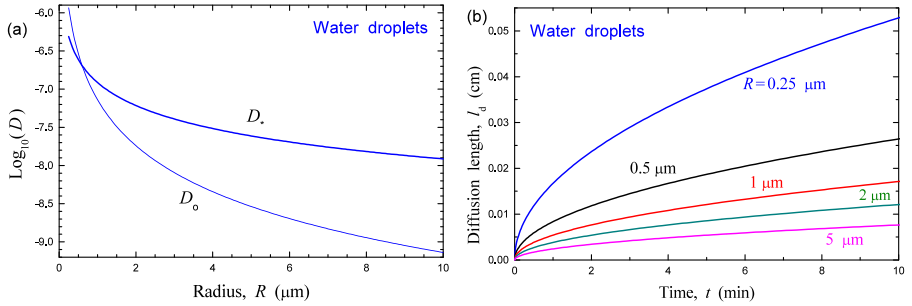

Fig. 2. As Fig. 1 for respiratory droplets. In this case, the fluid dynamics [Eq. (2)] is often more important than binary collisions.

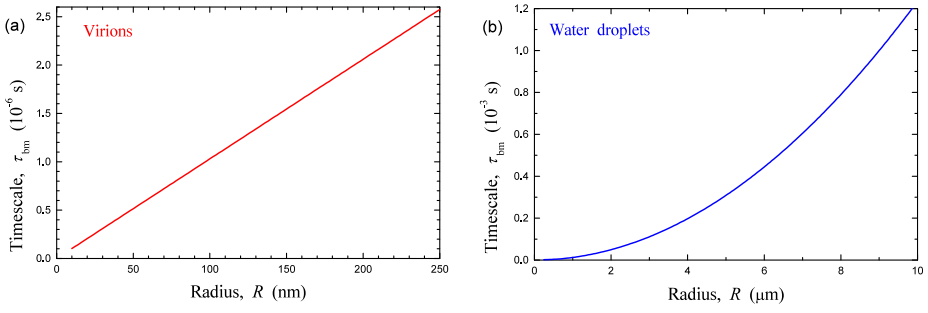

Fig. 3. Timescale of the ballistic motion [Eq. (12)] a function of radius of (a) virions (with $\rho = 1.4$ g/cm^3) and (b) respiratory droplets.

where

$$m = (4\pi/3)R^3\rho \tag{8}$$

is the particle mass (ρ is the density). The length of the ballistic motion is given by

$$l_{\mathrm{bm}} = \int_0^\infty v(0)\exp(-t/\alpha m)dt = \alpha m v(0). \tag{9}$$

These equations show that the timescale of the ballistic motion is determined by

$$\tau_{\mathrm{bm}} = \alpha m. \tag{10}$$

In addition, one should take into account that according to the detailed balance principle the mobility and diffusion coefficient [Eqs. (1)–(3)] are related as

$$\alpha = D/k_{\mathrm{B}}T. \tag{11}$$

Substituting (8) and (11) into (10) yields

$$\tau_{\mathrm{bm}} = \frac{4\pi\rho R^3 D}{3k_{\mathrm{B}}T} \tag{12}$$

Thus, $\tau_{\mathrm{bm}} \propto R$ if D is determined by (1), and $\tau_{\mathrm{bm}} \propto R^2$ if D is determined by (2). The scale of τ_{bm} is very short, shorter or about 3×10^{-6} s for virions and shorter or about 3×10^{-3} s for droplets (Fig. 3). l_{bm} is accordingly short as well. This means that the ballistic motion of single particles is practically negligible. This conclusion holds if one uses other more complex models and expressions for the force acting on particles (for such expressions, see, e.g., Chao and Wan, 2006; Goossens, 2019). It may occurs, however, collectively together with air (Section 3).

2.3. Gravity-induced motion of virions and droplets

Gravity induces the motion of virions and droplets in the vertical direction (along the z-coordinate). The corresponding force is $F_{\mathrm{g}} = mg$, where $g = 9.8$ m/s^2 is the acceleration of free fall. This force is counteracted by the fluid-dynamics friction force. If one neglects the latter force, the particle velocity and shift would depend on time as $v = gt$ and $\Delta z = gt^2/2$, and in terms of this shift the velocity would be represented as $v = (2g\Delta z)^{1/2}$. The friction force corresponding to this velocity would be $F_{\mathrm{h}} = (2g\Delta z)^{1/2}/\alpha = (2g\Delta z)^{1/2}k_{\mathrm{B}}T/D$. For practically interesting shifts, $\Delta z \sim 100$ cm, the latter force is a few orders of magnitude larger than F_{g} both for virions and respiratory droplets. This means that the situation is far from free fall, and the motion of these species in the direction under consideration should rather be viewed as the gravity-induced drift with the constant velocity and the

corresponding linear shift of the coordinate,

$$v = \alpha mg = mgD/k_BT, \tag{13}$$

$$\Delta z = vt = \alpha mgt = mgDt/k_BT. \tag{14}$$

This velocity is rather low (Fig. 4). In parallel with this drift, the particles also diffuse along the coordinate under consideration, and the corresponding 1D diffusion length is given by

$$l_d = (2Dt)^{1/2}. \tag{15}$$

This length is typically much shorter than the drift length (Fig. 5).

3. Ballistic motion with air

Sneezing, coughing, and talking induce and/or occur via air motion, and virions and respiratory droplets can move together with this air. The full-scale analysis of this motion should be based on numerical integration of the fluid-dynamics equations (see, e.g., Kao and Yang, 2006; Cho, 2019; Zhang et al., 2019; Busco et al., 2020; Dbouk and Drikakis, 2020a; Pendar and Pascoa, 2020; Wang et al., 2020a; for some of the less conventional pathways of virion propagation, see Sze To et al., 2009; Li et al., 2020; Wang et al., 2020b; Yang et al., 2020). Such calculations are beyond our goals. We rather aim at related estimates allowing one to understand what happens in this case or, more specifically, to estimate the time and length scales of relaxation of this motion. Roughly, we can consider that initially a spherical region of air with radius R_a and velocity v is generated in air which is stagnant outside this region. Then, the gas-phase molecules located initially in this region move in the direction of the initial velocity and simultaneously expand due to diffusion. The collective movement is terminated due to inter-diffusion and related friction. The mobility of or the force acting on the whole array of the molecules under consideration can be estimated by using the conventional Stokes model [as in (2)], i.e., $\alpha = 1/(6\pi\eta R_a)$ or $F = \alpha v = v/(6\pi\eta R_a)$ (Landau and Lifshitz, 1987). The corresponding air mass is equal to $m_a = (4\pi/3)R_a^3\rho_a$, where ρ_a is the air density. The timescale of relaxation of the motion can then be obtained by substituting these expressions for α and m_a into (10),

$$\tau_r = \frac{2\rho_a R_a^2}{9\eta}. \tag{16}$$

Concerning this expression and the estimates above, we can add that the Stokes model implies laminar flow (low Reynolds number). The corresponding expression for α or force can, however, be obtained by using scaling arguments irrespective of the value of the Reynolds number.

With $\rho_a = 1.2\times10^{-3}$ g/cm^3, $\eta = 1.8\times10^{-4}$ g/(s cm), and e.g. R_a = 2 cm, Eq. (16) yields $\tau_r = 6$ s. In reality, this timescale is shorter by a factor of about 3 due to expansion of the array of molecules, i.e., $\tau_r \simeq 2$ s. The scale of v during sneezing, coughing, and talking is 50–100 cm/s. The corresponding length scale is $l_a = v\tau_r \simeq$ 100–200 cm. This length known from everyday life and also from detailed fluid-dynamic calculations (see, e.g., Dbouk and Drikakis, 2020a) is behind the conventional recommendations concerning person–person distances needed to minimize infection. It corresponds to stagnant conditions. At wind speeds varying from 4 to 15 km/h, the respiratory droplets can travel up to 6 m in the wind direction (Dbouk and Drikakis, 2020a).

4. Evaporation of water from droplets

As already noticed in the Introduction, μm-sized respiratory droplets contain primarily water. The initial fraction of nonvolatile matter is there usually low, ≃0.01, but may be up to ≃0.05. Each droplet carrying virions can contain one, a few, or many virions. If a droplet is small whereas the number of virions is large (larger than 10), the total volume of virions can in principle be comparable or somewhat larger than the volume of nonvolatile matter. Often, however, the situation is opposite. Evaporation of water from droplets is often rapid on the timescale of diffusion and drift (Section 2) especially in dry air or at relatively high temperatures, and, as already noticed in the Introduction [see also e.g. recent studies by Vejerano and Marr, 2018 and Lin and Marr, 2020], this process is important in the context of transmission of infection via air. Roughly, the whole evaporation process can be divided into two stages. During the first (main) stage, the volume of water in a droplet is appreciably larger (at least by a factor of 2) than the volume of nonvolatile matter and virions, the effect of nonvolatile matter and virions on evaporation can be neglected, and the evaporation process can be described by employing the simplest textbook equations directly or with minor modifications (Section 4.1). During the second (late) stage, the volume of water is first comparable and then smaller than the volume of nonvolatile matter and virions, and the effect of nonvolatile matter and virions on evaporation should be taken into account (Section 4.2). In the context under consideration, some other aspects of evaporation are important as well (Sections 4.3 and 4.4).

4.1. Main stage of evaporation

During the main stage of evaporation, droplets contain primarily water. The air–droplet interface contains primarily water as well because the nonvolatile matter and virions are hydrophilic and have no tendency to segregate at the interface. Thus, as already noticed, the effect of nonvolatile matter and virions on evaporation can be neglected, and to describe this process one can use the classical Maxwell model [Sec. 4.2.1 in the monograph by Sazhin, 2014] implying that the gas-phase water molecules located near the air–water interface are in equilibrium with water in a droplet or, in other words, that the pressure of water in air near this interface is close to saturation, and the evaporation is controlled by diffusion of water molecules away from the interface. For spherically shaped droplets, the diffusion flux can easily be calculated, and then the corresponding balance equation for evaporation is represented as

$$\frac{4\pi R^2}{v_\circ}\frac{dR}{dt} = -4\pi R^2 \cdot D_* \frac{\Delta c}{R}, \tag{17}$$

where R is the droplet radius, $v_\circ$ is the volume per molecule in water, D_* is the diffusion coefficient of water molecules in air, and $\Delta c = c_s - c_\infty$ is the difference of the concentrations of water molecules in air near (at saturation) and far from a droplet, i.e., at $r = R$ and $r \gg R$ (r is the radial coordinate), respectively. The left-hand side of this equation describes the rate of evaporation in terms of the number of molecules in a droplet, whereas the right-hand side represents the same rate in terms of the diffusion flow. The equation does not take diffusion-induced convective air flow into account [cf. the Stefan-Fuchs model (Sazhin, 2014)]. This flow is, however, negligible, because the partial pressure of water in air is low compared to the atmospheric pressure. Dividing the left- and right-hand sides of this equation by $4\pi R^2/v_\circ$ yields

$$\frac{dR}{dt} = -v_\circ D_* \frac{\Delta c}{R}. \tag{18}$$

In applications of this equation in various fields of natural sciences in general (Sazhin, 2014) and in the context under consideration in particular (see, e.g., Chaudhuri et al., 2020), c_∞ is usually associated with the concentrations of gas-phase water molecules in air at the macroscopic scale, and Δc is considered to be constant. In the case of respiratory droplets, c_∞ should, however, be associated with the concentrations of gas-phase water molecules in the air flux generated during sneezing, coughing, or talking, and accordingly c_∞ depends on time even during the main stage of evaporation due to changing conditions in the air flux after its generation. With this reservation, it is instructive first to recall what happens if c_∞ and Δc are constant. Under such conditions, Eq. (18) results in the well-known R^2 law,

$$R^2(t) = R^2(0) - 2v_\circ D_* \Delta c\, t. \tag{19}$$

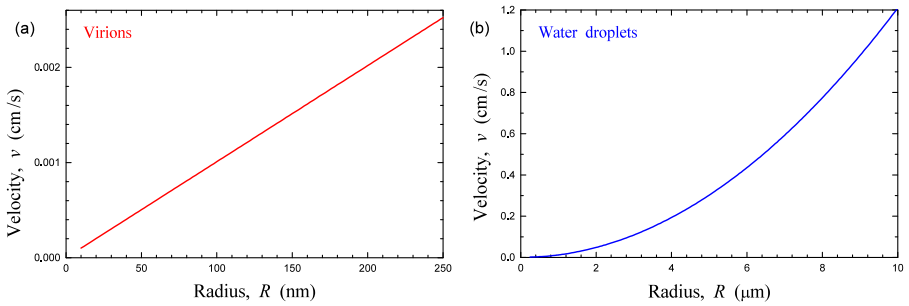

Fig. 4. Velocity of the gravity-induced drift of (a) virions and (b) respiratory droplets as a function of their radius [Eq. (13)].

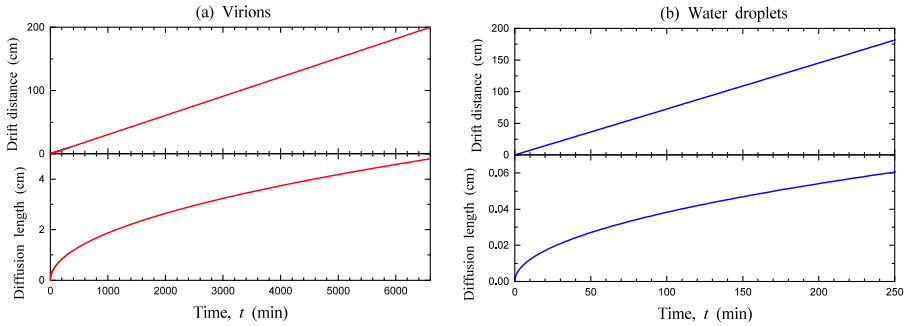

Fig. 5. Gravity-induced drift shift [Eq. (14)] and diffusion length [Eq. (15)] as a function of time for (a) 100-nm-sized virions and (b) 2-μm-sized respiratory droplets.

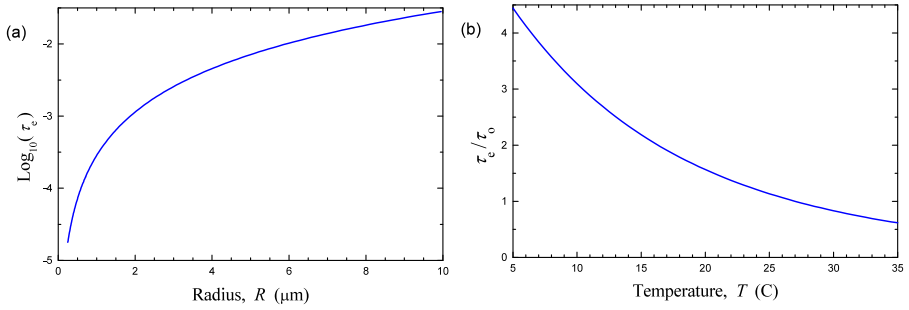

Fig. 6. Timescale of the fastest evaporation of water from respiratory droplets in dry air [Eq. (20)] (a) as a function of the droplet radius at $T = 300$ K, and (b) as a function of temperature. In the former case, the timescale is in s. In the latter case, the timescale is normalized to that at $T = 300$ K. [In the academic virus- or bacteria-related experiments focused on evaporation of water from water droplets, the size of droplets is usually much larger (see e.g. Lin and Marr, 2020).]

The corresponding timescale of evaporation, τ_e, can be associated with the moment when the droplet volume becomes half that of the initial one. In terms of the droplet radius, this condition means $R(\tau_e) = R(0)/2^{1/3}$. In combination with (19), it results in

$$\tau_e = \frac{0.19R^2(0)}{v_o D_* \Delta c} \equiv \frac{0.19R^2(0)}{v_o D_* (c_s - c_\infty)}. \tag{20}$$

Alternatively, this timescale can be defined as the time needed for evaporation of almost all water, i.e., by extrapolating $R(t)$ in (19) to zero,

$$\tau_e = \frac{R^2(0)}{2v_o D_* \Delta c} \equiv \frac{R^2(0)}{2v_o D_* (c_s - c_\infty)}. \tag{21}$$

In reality, the concentration of the gas-phase water molecules in the air flux just after its generation is expected to be close to saturation, i.e. $c_\infty \simeq c_s$, and accordingly the driving force for evaporation is negligible, $\Delta c(0) = c_s - c_\infty \simeq 0$. During propagation and expansion of the air flux, c_∞ decreases, Δc increases, and this facilitates evaporation. This effect can accurately be described only numerically (the corresponding references are given in Section 3). For estimates, it can be done at the level of the relaxation timescale, τ_r [Eq. (16) in Section 3] by using the simplest phenomenological equation for Δc,

$$\frac{d\Delta c}{dt} = (\Delta c_\star - \Delta c)/\tau_r \tag{22}$$

where $\Delta c_\star \equiv c_s - c_\infty^\star$ is the difference of the concentrations of water molecules in air at saturation and far from the air flux. With the suitable initial condition, $\Delta c(0) = 0$, this equation yields

$$\Delta c = \Delta c_\star [1 - \exp(-t/\tau_r)]. \tag{23}$$

Substituting this expression into Eq. (18), we have

$$R\frac{dR}{dt} = -v_o D_* \Delta c_\star [1 - \exp(-t/\tau_r)], \quad \text{or} \tag{24}$$

$$R^2 = R^2(0) - (2v_o D_* \Delta c_\star)(t - \tau_r[1 - \exp(-t/\tau_r)]). \tag{25}$$

If τ_r is short, $\tau_r[1 - \exp(-t/\tau_r)]$ can be neglected, and as expected we again obtain the conventional R^2 law [cf. (19)],

$$R^2(t) = R^2(0) - 2v_o D_* \Delta c_\star t. \tag{26}$$

If τ_r is long so that $t/\tau_r \ll 1$, $\exp(-t/\tau_r)$ can be expanded up to the second-order term, and we get

$$R^2(t) = R^2(0) - v_o D_* \Delta c_\star t^2/\tau_r. \tag{27}$$

This equation derived provided $t/\tau_r \ll 1$ predicts slower decrease of R compared to (26). The timescales of evaporation corresponding to Eqs. (26) and (27) can be defined by analogy with (20) and (21). In the case of Eq. (26), one should just replace Δc by $\Delta c_\star$ in (20) and (21). For Eq. (27), one can rewrite (20) and (21), respectively, as

$$\tau_e = \frac{0.61\tau_r^{1/2}R(0)}{(v_\circ D_* \Delta c_\star)^{1/2}} \equiv \frac{0.61\tau_r^{1/2}R(0)}{[v_\circ D_*(c_s - c_\infty^\star)]^{1/2}}, \tag{28}$$

$$\tau_e = \frac{\tau_r^{1/2}R(0)}{(v_\circ D_* \Delta c_\star)^{1/2}} \equiv \frac{\tau_r^{1/2}R(0)}{[v_\circ D_*(c_s - c_\infty^\star)]^{1/2}}. \tag{29}$$

To use the equations above, one needs an expression for c_s or related pressure, P_s, and an expression for D_*. Concerning c_s, one can notice that the infection-related water droplets contain nonvolatile matter, and it may influence the rate of water evaporation. The fraction of this matter is, however, low, and for estimates one can use c_s measured for pure water. One of the corresponding fairly accurate empirical expressions for P_s is (Richards, 1971)

$$P_s = P_* \exp(13.3185\kappa - 1.9760\kappa^2 - 0.6445\kappa^3 - 0.1299\kappa^4), \tag{30}$$

where $P_* \equiv 1.013\times10^5$ N/m^2, $\kappa \equiv 1\text{–}373.15/T$, and T is absolute ambient temperature (in K). A suitable expression for D_* is given in Table 2 in the article by Massman (1998), and the corresponding dependence of D_* on T is close to that in Eq. (1).

The timescale of evaporation calculated with the specification above for dry air and $T = 300$ K by employing Eq. (20) (with $c_\infty = 0$) is short (Fig. 6). With decreasing temperature under everyday life, it may increase by an order of magnitude. On the same scale, it can be increased with increasing air humidity (c_∞). At saturation, i.e. at $c_\infty \to c_s$, the evaporation becomes negligible. At oversaturation with $c_\infty > c_s$, respiratory droplets can play a role of nucleation centers and grow.

In fact, the evaporation timescale shown in Fig. 6 is shorter (especially for small droplets) than the timescale of relaxation of the air flux, $\tau_r \simeq 2$ s (as estimated in Section 3). This means that in reality the evaporation is often influenced by relaxation of the air flux.

4.2. Late stage of evaporation

During the late stage of evaporation of water from droplets, the volume of water is first comparable and then can become nearly equal to the volume of nonvolatile matter and virions. The volume of virions is smaller or may be comparable to that of nonvolatile matter. Virions are hydrophilic and can be considered to be located inside droplets. Under such conditions, the shape of droplets is expected to remain to be close to spherical, and the evaporation of water from droplets can still be described by Eq. (18) containing the concentration difference, $\Delta c = c_s - c_\infty$. The only difference is that now c_s corresponds to equilibrium of gas-phase water molecules with water in a droplet with appreciable fraction of the volume occupied by nonvolatile matter and virions (water is not in excess), this fraction depends on R, and accordingly Δc depends R as well, i.e., we have

$$\frac{dR}{dt} = -v_\circ D_* \frac{\Delta c(R)}{R}. \tag{31}$$

The calculation of the dependence of c_s or Δc on R is a prerogative of statistical physics. In the available models of evaporation from droplets containing the mixture of components [see, e.g., the monograph by Sazhin, 2014, recent articles by Fang et al., 2019, Narasu et al., 2020, and Chaudhuri et al., 2020, and references therein; for the related models focused on Ostwald ripening of alloyed nanoparticles, see, e.g., Alloyeau et al., 2010], $\Delta c(R)$ is calculated in various versions of the mean-field approximation implying that the components are distributed at random. In the context under consideration, this means that the nonvolatile matter does not aggregate in water. Taking the specifics of the nonvolatile matter into account (see the Introduction), this condition appears to be acceptable. In this framework, the dependence of Δc on R can be specified by using a few balance relations. The first one expresses the volume of water via the droplet radius as

$$V_w(R) = (4\pi/3)R^3 - V_{nm} - nV_v, \tag{32}$$

where $V_{nm} = (4\pi/3)R(0)^3 f$ is the volume of nonvolatile matter ($f \simeq 0.01\text{–}0.05$ is the fraction of this matter in a droplet at $t = 0$), V_v is the volume of a virion, and n is the number of virions. The second and third ones define the volume fraction of water in its mixture with nonvolatile matter,

$$\chi(R) = \frac{V_w(R)}{V_w(R) + V_{nm}} = \frac{(4\pi/3)R^3 - V_{nm} - nV_v}{(4\pi/3)R^3 - nV_v}, \tag{33}$$

and the volume fraction of nonvolatile matter in this mixture,

$$\xi(R) = \frac{V_{nm}}{V_w + V_{nm}} = \frac{V_{nm}}{(4\pi/3)R^3 - nV_v}. \tag{34}$$

With this specification, the mean-field approximation yields

$$\Delta c(R) = \chi(R)\exp[-B\xi(R)]c_s^\circ - c_\infty, \tag{35}$$

where c_s° is the concentration of water in air at saturation, $\chi(R)$ is the entropic factor defined by (34), and $B > 0$ is the parameter taking the interaction between water and nonvolatile matter into account.

Expression (35) contains two additional factors, $\chi(R) \le 1$ and $\exp[-B\xi(R)] \le 1$, reducing the water pressure near the interface compared to that, c_s°, corresponding to pure water. During the main stage of evaporation (Section 4.1), water in a droplet is in excess, both these factors are close to unity, and accordingly $c_s = c_s^\circ$. At the late state (with decreasing R), c_s is reduced and can become close to c_∞ provided the air is not dry ($c_\infty > 0$), and then the evaporation of water will be terminated.

If the air is dry ($c_\infty^\star = 0$), the evaporation of water may occur up to the end, i.e., up to the stage when a droplet contains only nonvolatile matter and virions. The simplest corresponding kinetics can be described by assuming the relaxation of the air flux to be rapid and using the equation obtained by substituting (35) with $c_\infty = 0$ into (31), i.e.,

$$\exp[B\xi(R)]\frac{R}{\chi(R)}\frac{dR}{dt} = -\frac{R^2(0)}{2\tau_e}, \tag{36}$$

where τ_e is the timescale defined by (21) (with $c_s = c_s^\circ$ and $c_\infty = 0$). According to this equation, the square of the droplet radius decreases linearly with increasing time up to $t \simeq \tau_e$ (Fig. 7) as earlier already been shown [Eq. (19)]. Then, there is rapid transition to the state where the water content in a droplet is negligible and its size is constant.

As already noticed, Eqs. (35) and (36) imply that the components are distributed in a droplet at random, i.e., there is no aggregation of the nonvolatile matter. In addition, (i) the diffusion of this matter should be fast on the timescale of evaporation [i.e., the diffusion length formally estimated on this time scale by using Eq. (15) should be larger than the droplet size] or at least (ii) the fraction of this matter should be low. For the main (e.g., non-organic) components of saliva (see the Introduction), condition (i) holds. The diffusion of biological molecules (proteins and enzymes) is relatively slow, but the fraction of volume they occupy is very low [the protein content in saliva is, e.g., ≃1.3 mg/ml (Sarkar et al., 2019)], and accordingly condition (ii) is expected to hold. The diffusion of virions is slow, but the fraction of volume their occupy is very low as well, i.e., condition (ii) is fulfilled. If the fraction of the droplet volume occupied by slow diffusing matter is appreciable, the distribution of this matter changes during evaporation, and accordingly Eqs. (35) and (36) are not applicable. For general readership, we may mention that the latter scenario was analyzed in many articles (Charlesworth and Marshall, 1960; Abdullahi et al., 2020).

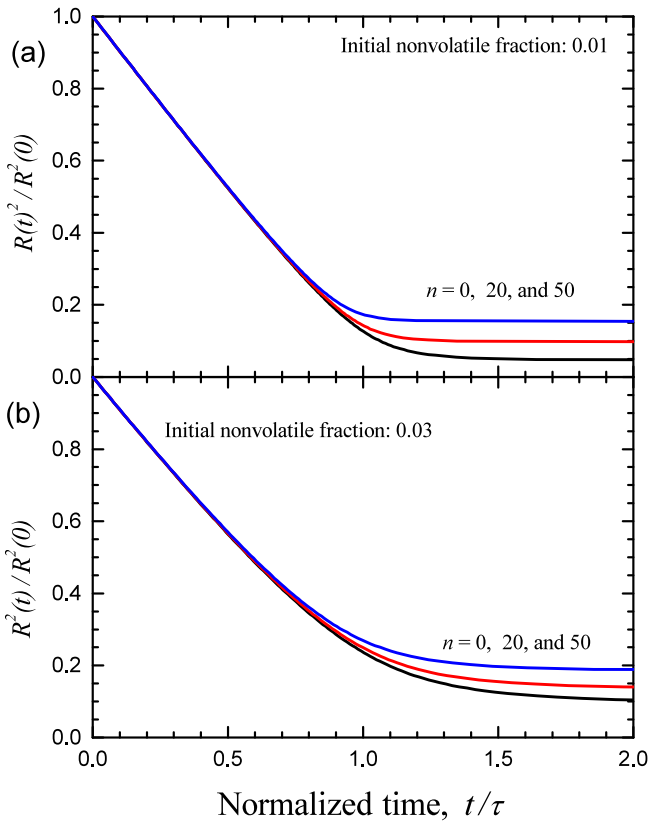

Fig. 7. Square of the droplet radius as a function of time for droplets with $R(0) = 0.5$ μm and $f = 0.01$ (a) and 0.03 (b). Three curves correspond to $N_v = 0$, 20, and 50. The virion size (diameter) is 100 nm (this value corresponds to influenza virus). The results were obtained by using Eq. (36) with $B = 2$. This value of B corresponds to the situation when the nonvolatile matter does not aggregate in water.

4.3. Drift and evaporation

For the water droplets under consideration, the timescale of evaporation is much shorter than that characterizing their gravity-induced drift towards the flow [cf. Fig. 5(b) and 6]. This means that the analysis of the drift presented in Section 2.3 is incomplete because the drift is there neglected. To extend the analysis, we take into account that $m \propto R^3$ [Eq. (8)], adopt the simplest dependence of the droplet diffusion coefficient on radius, $D \propto 1/R$ [Eq. (2)], and rewrite Eq. (13) as $dz/dt = -AR^2(t)$, where $A = (2/9)\rho g/\eta$ is the properly defined constant. If for example $R^2(t)$ is given by (19), we then have

$$dz/dt = -A[R^2(0) - 2v_\circ D_* \Delta c\, t], \quad \text{or} \tag{37}$$

$$z = -At[R^2(0) - v_\circ D_* \Delta c\, t]. \tag{38}$$

Using again (19) for $R^2(t)$, the latter equation can be represented in an alternative form as

$$z = -At[R^2(t) + v_\circ D_* \Delta c\, t]. \tag{39}$$

These equations or similar equations obtained by using Eq. (27) for $R^2(t)$ show that the time dependence of the shift, $z(t)$, is not determined solely by $R^2(0)$, and that without taking evaporation into account, the measurements of this shift cannot be used in order to determine $R(0)$.

4.4. Related aspects

The analysis above is focused on evaporation of water from respiratory droplets migrating in air. Such droplets can contact and stick to solid surfaces, and then the evaporation may occur as well. The models described above can easily be extended to this case by taking the corresponding change of the droplet shape into account. The models of this category (without inclusion of the effect of nonvolatile matter and virions on the evaporation rate) have recently been employed by Bhardwaj and Agrawal (2020a,b).

Another more complex situation takes place when respiratory droplets are carried by air through a face mask. The corresponding droplet dynamics have recently been analyzed by Dbouk and Drikakis (2020b) taking into account turbulent dispersion forces, droplet phase-change, evaporation (without inclusion of the effect of nonvolatile matter and virions on the evaporation rate), and breakup in addition to the droplet–droplet and droplet–air interactions. The results obtained have allowed them to scrutinize the criteria for assessing the face mask performance. The state of the art of the related experiments can be learned from the recent articles by Konda et al. (2020) and Verma et al. (2020).

5. After attachment to the epithelium

5.1. General remarks

Via diffusion and drift in air, virions and/or μm-sized virion-carrying droplets may reach the epithelial cells forming the respiratory mucosa and start the viral cycle inside these or underlying cells. One of the key basic question here is how large is the minimal number of virions needed for the initiation of infection in a host? Customarily, this question was long addressed by determining the minimum infective dose (MID) in experiments employing assays with monolayers of cells where the viral doses are expressed either as the dilution of virus sufficient to cause cytopathic effect in 50% of the inoculated culture ($TCID_{50}$) or as plaque-forming units [pfu; reviewed by Yezli and Otter, 2011; see also the article by Mistry et al., 1918 for a related statistical model]. In such measurements, the total number of virions is, however, usually not exactly known, and the minimal number of virions needed really for initiation cannot be inferred. More advanced experiments performed with non-human viruses indicate that some of the infections can be induced by one virion [Zwart et al., 2009 and Zwart et al., 2011; reviewed by Zwart and Elena, 2015]. Often, however, the minimal number of virions is believed to be larger than one (Sanjuán, 2017, 2018). The extent to which these conclusions are applicable to humans in general and to respiratory infections such e.g. as influenza or COVID-19 in particular has, however, not yet been firmly established [concerning influenza, see, e.g., recent experiments by Ramos et al., 2019; concerning COVID-19, see, e.g., the discussion by Stadnytskyi et al., 2020].

Many related experimental and theoretical studies are focused on the mechanistic aspects of the initiation of infections or, more specifically, on the entry of single virions into the host cells (see e.g. Cossart and Helenius, 2014; Zhdanov, 2015, respectively, and references therein). There are also simulations of virion diffusion along the epithelium and penetration into the epithelium cells (Beauchemin et al., 2006; Segredo-Otero and Sanjuán, 2020; Whitman et al., 2020). One of the theoretical studies is focused on the balance between virion attachment to and detachment from the membrane of a cell and virion transitions into and from a cell under steady-state conditions with respect to the external virion concentration (Handel et al., 2014). All these models (Beauchemin et al., 2006; Segredo-Otero and Sanjuán, 2020; Whitman et al., 2020; Handel et al., 2014) and the models aimed at intracellular viral kinetics [reviewed by Yin and Redovich, 2018 and Zhdanov, 2018] are, however, not directly applicable to the interaction of virion-carrying droplets with the epithelium because the initial virion distributions used there do not correspond to that related to droplets. The understanding of what happens in the very beginning of respiratory infections when virion-carrying droplets interact with the epithelial cells is still limited. We discuss the corresponding physical and biological aspects below in Section 5.2 and in Sections 5.3 and 5.4, respectively.

5.2. Virions in the mucus and periciliary layers

The epithelial cells form a layer separated from the cells located deeper by the basement membrane representing a dense, highly cross-linked, sheet-like extracellular matrix (Kelley et al., 2014; de Vries et al., 2020). Virions penetrate a gel-like mobile mucus layer as well as a brush-like periciliary layer located above the epithelium and contact the epithelial cells (de Vries et al., 2020). Due to close-packing of epithelial cells and the presence of the basement membrane, the contacts of virions with the deeper-located cells are hampered. For this reason, just after arrival, the virions diffuse along the layer of epithelial cells and this process is accompanied by detachment, degradation, and the membrane penetration. At the solution-cell-membrane interface, diffusion of virions and other biological nanoparticles with size $\sim$ 100 nm is controlled by their flexible ligand–receptor links with the membrane. If the number of these links, n, is small and they are durable, the scale of the diffusion coefficient is 0.2 $\mu m^2/s$ (Block et al., 2016). With increasing n, the diffusion coefficient decreases in this case approximately as $\propto 1/n$ (Block et al., 2016). Alternatively, a virion can diffuse as a spider via rupture and formation of ligand–receptor pairs (Hamming et al., 2020). The diffusion can be influenced by the membrane-spanning mucins (proteins) forming the carcass of the periciliary layer (de Vries et al., 2020). The full-scale information about the rates of this diffusion *in vivo*, as well as about virion detachment, degradation, and penetration the epithelial-cell membrane is yet lacking.

In the case of a single virion, the probability to get into a cell after its attachment to the cell membrane is

$$P = k_p/(k_p + k_d + k_*), \tag{40}$$

where k_p, k_d, and k_* are the penetration, detachment, and degradation rate constants. This probability can be identified with the infection probability provided one virion is sufficient for the initiation of infection.

A μm-sized respiratory virion-containing droplet is able to deliver a few or many virions to the area comparable to the cell cross-section. To estimate the average number of virions penetrating the membrane of the cells contacting a droplet after its attachment, we can consider that just after its contact with the epithelium the virions are distributed in the mucus and periciliary layers as

$$c(r,0) = \frac{N_v}{\pi r_\circ^2}\exp\left(-\frac{r^2}{r_\circ^2}\right), \tag{41}$$

where N_v is the number of virions [as n in (32)], r is the 2D radial coordinate ($r = 0$ corresponds to the center of the contact region), and $r_\circ$ is the length scale characterizing the virion distribution. This physically reasonable initial distribution is expected to be valid provided virions do not aggregate. Its shape is mathematically convenient because it coincides with the Green function for 2D diffusion (Zhdanov, 1991), and accordingly its evolution is given by

$$c(r,t) = \frac{N_v}{\pi(r_\circ^2 + 4Dt)}\exp\left(-\frac{r^2}{r_\circ^2 + 4Dt} - (k_p + k_d + k_*)t\right), \tag{42}$$

where D is the effective coefficient of virion diffusion in the lumped layer including the mucus and periciliary layers.

The probability of infection of a cell increases with increasing the number of absorbed virions. Thus, the cell located in the center of the contact area has the highest probability of infection. For such cells, the rate of absorption of virions is given by

$$w(t) = k_p\int_0^R c(r,t)2\pi r dr, \tag{43}$$

where R is the radius of the area corresponding to a single cell at the epithelium. Substituting (42) into (43) yields

$$w(t) = k_p N_v\left[1 - \exp\left(-\frac{R^2}{r_\circ^2 + 4Dt}\right)\right]\exp[-(k_p + k_d + k_*)t]. \tag{44}$$

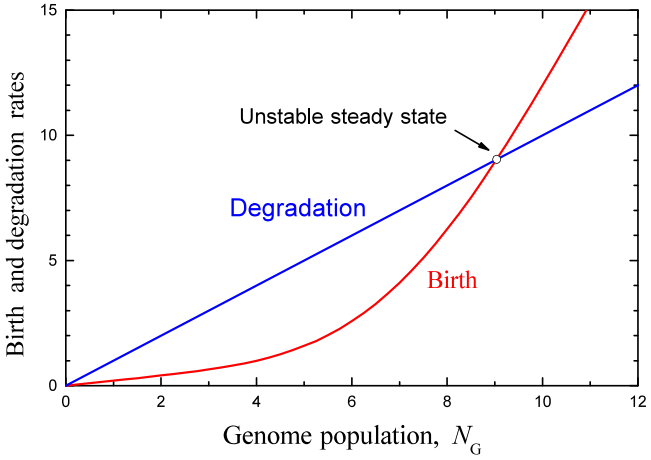

Fig. 8. Graphical solution of Eq. (52) with positive feedback for replication [Eq. (51) with $k_r^\circ/\kappa_G = 0.2$, $k_r^*/\kappa_G = 2$, $K = 10$, and $m = 4$] and no feedback for degradation under steady-state conditions [with $w(t) = 0$]. The virion birth and degradation rates are normalized to κ_G.

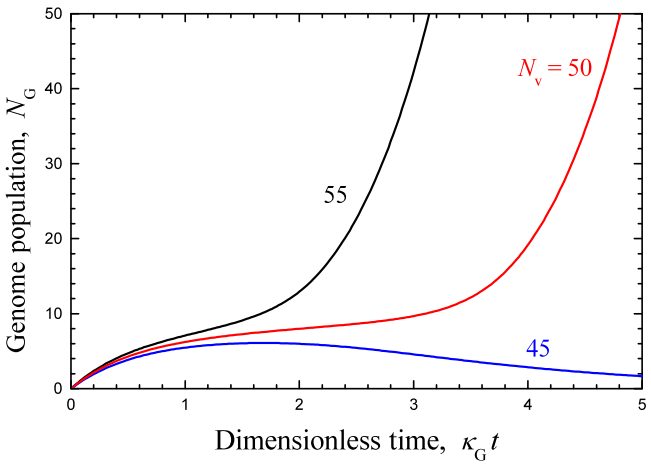

Fig. 9. Number of virions in a cell as a function of time according to Eq. (52) with positive feedback for replication [Eq. (51) with the same parameters as those used to construct Fig. 8]. The supply of virions is described by employing Eq. (46) with $k_p/\kappa_G = 0.5$, $k_d = k_* = 0$, $r_\circ^2/R^2 = 2$, and $4D/R^2\kappa_G = 0.5$. Three kinetics are shown for $N_v = 45$, 50, and 55, respectively.

This expression can be simplified in two limits. If $R \gg r_\circ$, $\exp[-R^2/(r_\circ^2 + 4Dt)]$ can be neglected, and we have

$$w(t) \simeq k_p N_v \exp[-(k_p + k_d + k_*)t]. \tag{45}$$

In the opposite limit with $R \ll r_\circ$, the exponential function in (44) can be expanded as $\exp[-R^2/(r_\circ^2 + 4Dt)] \simeq 1 - R^2/(r_\circ^2 + 4Dt)$, and we obtain

$$w(t) \simeq \frac{k_p N_v R^2}{r_\circ^2 + 4Dt}\exp[-(k_p + k_d + k_*)t]. \tag{46}$$

The total number of virions absorbed by a cell is defined by

$$N_{ab} = \int_0^\infty w(t)dt. \tag{47}$$

This expression can also be easily simplified in various limits.

5.3. Compensation of genetic and/or structural virion defects

The analysis above illustrates that the very initial interaction of virions with cells after their diffusion in air alone or inside respiratory droplets depends on many factors and is kinetically not simple. It can,

however, be described analytically, and the corresponding equations can be used as a basis for scrutinizing the intracellular viral kinetics with the droplet-mediated supply of virions. The important point here is that each respiratory droplet can deliver a few or many virions into a cell. By analogy with the viral transmission including virion aggregation or occurring with participation of exosomes (Sanjuán, 2018), this feature may be favorable for infection because it may compensate intrinsic genetic and/or structural virion defects or help to overcome host infection barriers that limit early viral proliferation (e.g., replication). The former is expected be important in the case of segmented viruses such e.g as influenza A [Phipps et al., 2020; the corresponding genome consists of eight single-stranded viral RNA segments contained in separate viral ribonucleoprotein complexes that are packaged together into a single virion (Dadonaite et al., 2019)]. The latter may be important in the case of single-stranded RNA viruses such as COVID 19 (for its structure, see e.g. Wu et al., 2020 and Zhang and Kutateladze, 2020).

Theoretically, the effect of genetic complementation on the fitness and diversity of viruses spreading as collective infectious units have recently been analyzed by Segredo-Otero and Sanjuán (2018). They have shown that complementation among co-spreading viruses initially buffers the deleterious effects of mutations, but has no positive effect on mean population fitness over the long term, and even promotes error catastrophe at high mutation rates.

5.4. Overcoming the limitations in early viral replication

The models aimed at intracellular viral kinetics are numerous (Yin and Redovich, 2018; Zhdanov, 2018). In the simplest course-grained model describing how barriers can limit early replication of viral genomes (e.g., the RNA strands), G, the replication step can be represented as (Zhdanov, 2005)

$$\mathrm{G} \rightarrow 2\mathrm{G}, \tag{48}$$

and the corresponding equation for the G population is as follows

$$dN_{\mathrm{G}}/dt = k_{\mathrm{r}}(N_{\mathrm{G}})N_{\mathrm{G}} - \kappa_{\mathrm{G}}(N_{\mathrm{G}})N_{\mathrm{G}} + w(t), \tag{49}$$

where $w(t)$ is the supply rate defined by (44), and $k_{\mathrm{r}}(N_{\mathrm{G}})$ and $\kappa_{\mathrm{G}}(N_{\mathrm{G}})$ are the replication and degradation rate constants. These rate constants are considered to depend on N_{G} due to the feedback related to the interplay of various host and viral RNAs and proteins (the corresponding steps are usually rapid on the replication time scale and not described here explicitly).

If the virion population is small so that the feedback is negligible, the replication and degradation rate constants can be considered to be independent of N_{G}, i.e., $k_{\mathrm{r}}(N_{\mathrm{G}})$ and $\kappa_{\mathrm{G}}(N_{\mathrm{G}})$ can be replaced by $k_{\mathrm{r}}(1)$ and $\kappa_{\mathrm{G}}(1)$. In this limit, Eq. (49) can be rewritten as

$$dN_{\mathrm{G}}/dt = k_{\mathrm{r}}(1)N_{\mathrm{G}} - \kappa_{\mathrm{G}}(1)N_{\mathrm{G}} + w(t). \tag{50}$$

After termination of the supply [e.g., with $w(t) = 0$], the latter equation predicts exponential growth provided $k_{\mathrm{r}}(1) > \kappa_{\mathrm{G}}$ and extinction provided $k_{\mathrm{r}}(1) < \kappa_{\mathrm{G}}$.

The feedback can be described phenomenologically by using the Hill expressions for the replication and/or degradation rate constants [this approach is widely employed in the kinetic models of gene expression (Zhdanov, 2011)]. In this framework with, for example, positive feedback for replication (k_{r}°, k_{r}^{*}, K, and m are the corresponding parameters),

$$k_{\mathrm{r}}(N_{\mathrm{G}}) = k_{\mathrm{r}}^{\circ} + \frac{k_{\mathrm{r}}^{*}N_{\mathrm{G}}^{m}}{K^{m} + N_{\mathrm{G}}^{m}}, \tag{51}$$

and no feedback for degradation (κ_{G} is constant), Eq. (49) is represented as

$$dN_{\mathrm{G}}/dt = k_{\mathrm{r}}(N_{\mathrm{G}})N_{\mathrm{G}} - \kappa_{\mathrm{G}}N_{\mathrm{G}} + w(t). \tag{52}$$

Under steady-state conditions [with $w(t) = 0$], Eq. (52) in combination with (51) predicts the existence of a unstable steady state (Fig. 8) controlling the transition from extinction to exponential growth. The corresponding transient kinetics (Fig. 9), calculated with $w(t)$ given by (46), exhibit what happens with increasing the number of virions, N_{v}, in a droplet. With the parameter values chosen, the full-scale infection of the cell does not happen if $N_{\mathrm{v}} < 50$. For $N_{\mathrm{v}} \geq 50$, the growth of the virion populations is first slow [this slowdown is a general feature of the kinetics occurring near a unstable steady state (Zhdanov, 2019)] and then becomes exponential. The latter corresponds to full-scale infection of a cell. Thus, in the example under consideration, a droplet should contain at least 50 virions in order to be efficient in infection. This number can be identified with the minimal number of virions needed for the initiation of infection. Some of the virions located initially in a droplet are, however, not absorbed by the cell under consideration. For this reason, the definition of the minimal number of virions needed for infection of a cell is not unique. Another also reasonable definition is to identify this number with the minimal number of absorbed virions. In the example presented, the latter number is 18.

In the example above, the minimal numbers of virions were obtained by using the mean-field kinetic equations. If one takes fluctuations into account (e.g., by employing the Monte Carlo technique), the full-scale infection of cells may happen if N_{v} is slightly smaller than 50 or not happen if N_{v} is slightly larger than 50. The minimal number of virions absorbed by a cell may be slightly smaller or larger than 18 as well. Thus, the introduced minimal numbers of virions for initiation are on average equal to 50 and 18.

This theoretical analysis shows mechanistically at the coarse-grained level why the local droplet-mediated supply of an appreciable number of virions can be favorable for the initiation of infection.

6. Conclusion

We have (i) systematically described the behavior of virions and virion-carrying respiratory droplets in air with emphasis on diffusion, drift, and evaporation and (ii) estimated the rates of these steps. The key conclusions illustrated quantitatively are as follows:

- Under stagnant conditions, diffusion and drift of virions and respiratory droplets of the size typical for transport of virions is fairly slow. For example, it may take hours to reach a floor or land.
- Evaporation of water from droplets is fairly rapid. In dry air, it occurs up to the state when droplets contain primarily nonvolatile matter and virions. The main stage of evaporation does not depend on nonvolatile matter and virions.
- The rate of net-evaporation can decrease by order of magnitude with increasing humidity or decreasing temperature. At saturation (100 percent humidity) and oversaturation, the evaporation is negligible or the respiratory droplets may grow, respectively.
- Evaporation of water appreciably influences diffusion and drift of droplets which in turn means that the latter processes strongly depend on temperature and humidity due to evaporation.
- Convective air-flux-mediated transport of virions and droplets is rapid and can easily reach distances up to a few meters.

In addition, we have briefly discussed and analyzed the kinetic aspects of the first step of infection after attachment of virions or respiratory virion-carrying droplets to the epithelium. The corresponding conclusions are as follows:

- The kinetics of trapping of virions and the number of virions trapped by cells after attachment of a respiratory droplet to the epithelium depends on various rate constants. Although the values of these rate constants are yet lacking, the analysis predicts that the dependence of the rate of the virion supply to a cell on time should be exponential or exponential with the reciprocal correction.
- In general, the minimal number of virions needed for the initiation of infection in a cell is expected to be dependent on the feedback in the early intracellular viral-genome replication and can be appreciable. In

addition, simultaneous delivery of a few or many virions into a cell may compensate intrinsic genetic and/or structural virion defects. The supply of virions by respiratory droplets appears to be efficient from these perspectives. This may be one of the reasons why the infections (e.g., influenza and COVID 19) transmitted via air during sneezing, coughing, and talking are often easily propagating.

• Additional theoretical and experimental work is required to better understand the mechanistic aspects of the initiation of infection by virion-carrying respiratory droplets.

Declaration of competing interest

The authors declare that they have no known competing financial interests or personal relationships that could have appeared to influence the work reported in this paper.

References

Abdullahi, H., Burcham, C.L., Vetter, T., 2020. A mechanistic model to predict droplet drying history and particle shell formation in multicomponent systems. Chem. Eng. Sci. 224, 115713.

Alloyeau, D., et al., 2010. Ostwald ripening in nanoalloys: When thermodynamics drives a size-dependent article composition. Phys. Rev. Lett. 105, 255901.

Altan-Bonnet, T., 2016. Extracellular vesicles are the Trojan horses of viral infection. Curr. Opin. Microbiol. 32, 77–81.

Altan-Bonnet, G., Mora, T., Walczak, A.M., 2020. Quantitative immunology for physicists. Phys. Rep. 849, 1–83.

Andreu-Moreno, I., Sanjuán, R., 2020. Collective viral spread mediated by virion aggregates promotes the evolution of defective interfering particles. mBio 11, e02156-19.

Beauchemin, C., Forrest, S., Koster, F.T., 2006. Modeling influenza viral dynamics in tissue. In: Bersini, H., Carneiro, J. (Eds.), Artificial Immune Systems. Springer, Berlin, pp. 23–36.

Bertozzi, A.L., Franco, E., Mohler, G., Short, M.B., Sledge, D., 2020. The challenges of modeling and forecasting the spread of COVID-19. Proc. Natl. Acad. Sci. USA 117, 16732–16738.

Bhardwaj, R., Agrawal, A., 2020a. Likelihood of survival of coronavirus in a respiratory droplet deposited on a solid surface. Phys. Fluids 32, 061704.

Bhardwaj, R., Agrawal, A., 2020b. Tailoring surface wettability to reduce chances of infection of COVID-19 by a respiratory droplet and to improve the effectiveness of personal protection equipment. Phys. Fluids 32, 081702.

Block, S., Zhdanov, V.P., Höök, F., 2016. Quantification of multivalent interactions by tracking single biological nanoparticle mobility on a lipid membrane. Nano Lett. 16, 4382–4390.

Bocharov, G., Volpert, V., Ludewig, B., Meyerhans, A., 2018. Mathematical Immunology of Virus Infections. Springer, Cham.

Bou, J.V., Geller, R., Sanjuán, R., 2019. Membrane-associated enteroviruses undergo intercellular transmission as pools of sibling viral genomes. Cell Rep. 29, 714–723.

Busco, G., Yang, S.R., Seo, S., Hassan, Y.A., 2020. Sneezing and asymptomatic virus transmission. Phys. Fluids 32, 073309.

Chao, C.Y.H., Wan, M.P., 2006. A study of the dispersion of expiratory aerosols in unidirectional downward and ceiling-return type airflows using a multiphase approach. Indoor Air 16, 296–312.

Charlesworth, D.H., Marshall, W.R., 1960. Evaporation from drops containing dissolved solids. AIChE J. 6, 9–23.

Chaudhuri, S., Basu, S., Kabi, P., Unni, V.R., Saha, A., 2020. Modeling the role of respiratory droplets in Covid-19 type pandemics. Phys. Fluids 32, 063309.

Cho, J., 2019. Investigation on the contaminant distribution with improved ventilation system in hospital isolation rooms: Effect of supply and exhaust air diffuser configurations. Appl. Therm. Eng. 148, 208–218.

Cossart, P., Helenius, A., 2014. Endocytosis of viruses and bacteria. Cold Spring Harbor Perspect. Biol. 6, a016972.

Dadonaite, B., et al., 2019. The structure of the influenza A virus genome. Nat. Microbiol. 4, 1781–1789.

Dbouk, T., Drikakis, D., 2020a. On coughing and airborne droplet transmission to humans. Phys. Fluids 32, 053310.

Dbouk, T., Drikakis, D., 2020b. On respiratory droplets and face masks. Phys. Fluids 32, 063303.

De-Leon, H., Pederiva, F., 2020. Particle modeling of the spreading of coronavirus disease (COVID-19). Phys. Fluids 32, 087113.

de Vries, E., Du, W., Guo, H., de Haan, C.A.M., 2020. Influenza A virus hemagglutinin-neuraminidase-receptor balance: Preserving virus motility. Trends Microbiol. 28, 57–67.

Erickson, A.K., Jesudhasan, P.R., Mayer, M.J., Narbad, A., Winter, S.E., Pfeiffer, J.K., 2018. Bacteria facilitate enteric virus vo-infection of mammalian cells and promote genetic recombination. Cell Host Microbe 23, 77–88.

Fabricius, G., Maltz, A., 2020. Exploring the threshold of epidemic spreading for a stochastic SIR model with local and global contacts. Physica A 540, 123208.

Fang, B., Chen, L., Li, G., Wang, L., 2019. Multi-component droplet evaporation model incorporating the effects of non-ideality and thermal radiation. Int. J. Heat Mass Transfer 136, 962–971.

Gao, D., van den Driessche, P., Cosner, C., 2019. Habitat fragmentation promotes malaria persistence. J. Math. Biol. 79, 2255–2280.

Goossens, W.R.A., 2019. Review of the empirical correlations for the drag coefficient of rigid spheres. Powder Technol. 352, 350–359.

Goyal, A., Liao, L.E., Perelson, A.S., 2019. Within-host mathematical models of hepatitis b virus infection: Past, present, and future. Curr. Opin. Syst. Biol. 18, 27–35.

Gralton, J., Tovey, E., McLaws, M.-L., Rawlinson, W.D., 2011. The role of particle size in aerosolised pathogen transmission: A review. J. Infect. 62, 1–13.

Hamming, P.H., Overeem, N.J., Huskens, J., 2020. Influenza as a molecular walker. Chem. Sci. 11, 27–36.

Handel, A., Akin, V., Pilyugin, S.S., Zarnitsyna, V., Antia, R., 2014. How sticky should a virus be? The impact of virus binding and release on transmission fitness using influenza as an example. J. R. Soc. Interface 11, 20131083.

Handel, A., La Gruta, N.L., Thomas, P.G., 2020. Simulation modelling for immunologists. Nat. Rev. Immun. 20, 186–195.

Haseltine, E.L., Rawlings, J.B., Yin, J., 2005. Dynamics of viral infections: Incorporating both the intracellular and extracellular levels. Comput. Chem. Eng. 29, 675–686.

Huang, C., et al., 2020. Clinical features of patients infected with 2019 novel coronavirus in Wuhan, China. Lancet 395, 497–506.

Humphrey, S.P., Williamson, R.T., 2001. A review of saliva: normal composition, flow, and function. J. Prosthet. Dent. 85, 162–169.

Jefferys, E.E., Sansom, M.S.P., 2019. Computational virology: Molecular simulations of virus dynamics and interactions. In: Greber, U.F. (Ed.), Physical Virology, Virus Structure and Mechanics. Springer, Cham, pp. 201–233.

Kao, P.H., Yang, R.J., 2006. Virus diffusion in isolation rooms. J. Hosp. Infect. 62, 338–345.

Kelley, L.C., Lohmer, L.L., Hagedorn, E.J., Sherwood, D.R., 2014. Traversing the basement membrane in vivo: A diversity of strategies. J. Cell Biol. 204, 291–302.

Konda, A., Prakash, A., Moss, G.A., Schmoldt, M., Grant, G.D., Guha, S., 2020. Aerosol filtration efficiency of common fabrics used in respiratory cloth masks. ACS Nano 14, 6339–6347.

Landau, L.D., Lifshitz, E.M., 1987. Fluid Mechanics. Pergamon Press, Oxford.

Leeks, A., Sanjuán, R., West, S.A., 2019. The evolution of collective infectious units in viruses. Virus Res. 265, 94–101.

Li, S., Eghiaian, F., Sieben, C., Herrmann, A., Schaap, I.A.T., 2011. Bending and puncturing the influenza lipid envelope. Biophys. J. 100, 637–645.

Li, Y.-Y., Wang, J.-Y., Chen, X., 2020. Can a toilet promote virus transmission? From a fluid dynamics perspective. Phys. Fluids 32, 065107.

Lifshitz, E.M., Pitaevskii, L.P., 1981. Physical Kinetics. Pergamon Press, Oxford.

Lin, K., Marr, L.C., 2020. Humidity-dependent decay of viruses, but not bacteria, in aerosols and droplets follows disinfection kinetics. Environ. Sci. Technol. 54, 1024–1032.

Marijnissen, J.C.M., Gradoń, L. (Eds.), 2010. Nanoparticles in Medicine and Environment: Inhalation and Health Effects. Springer, Dordrecht.

Massman, W.J., 1998. A review of the molecular diffusivities of H_2O, CO_2, CH_4, CO, O_3, SO_2, NH_3, N_2O, NO, and NO_2 in air, O_2 and N_2 near STP. Atmos. Environ. 32, 1111–1127.

Mistry, B.A., D'Orsogna, M.R., Chou, T., 1918. The effects of statistical multiplicity of infection on virus quantification and infectivity assays. Biophys. J. 114, 2974–2985.

Morawska, L., et al., 2009. Size distribution and sites of origin of droplets expelled from the human respiratory tract during expiratory activities. Aerosol Sci. 40, 256–269.

Moskal, A., Sosnowski, T.R., Gradoń, L., 2010. Inhalation and deposition of nanoparticles: Fundamentals, phenomenology and practical aspects. In: Marijnissen, J.C.M., Gradoń, L. (Eds.), Nanoparticles in Medicine and Environment: Inhalation and Health Effects. Springer, Dordrecht, pp. 113–144.

Narasu, P., Boschmann, S., Pöschko, P., Zhao, F., Gutheil, E., 2020. Modeling and simulation of single ethanol/water droplet evaporation in dry and humid air. Comb. Sci. Technol. 192, 1233–1252.

Pendar, M.-R., Pascoa, J.C., 2020. Numerical modeling of the distribution of virus carrying saliva droplets during sneeze and cough. Phys. Fluids 32, 083305.

Phipps, K.L., et al., 2020. Collective interactions augment influenza a virus replication in a host-dependent manner. Nat. Microbiol. 5, 1158–1169.

Ramos, I., et al., 2019. Innate immune response to influenza virus at single-cell resolution in human epithelial cells revealed paracrine induction of interferon lambda 1. J. Virol. 93, e00559-19.

Richards, J.M., 1971. A simple expression for the saturation vapour pressure of water in the range -50 to 140 °c. J. Phys. D: Appl. Phys. 4, L15.

Sanjuán, R., 2017. Collective infectious units in viruses. Trends Microbiol. 25, 402–412.

Sanjuán, R., 2018. Collective properties of viral infectivity. Curr. Opin. Virol. 2018, 1–6.

Sarkar, A., Xua, F., Lee, S., 2019. Human saliva and model saliva at bulk to adsorbed phases - similarities and differences. Adv. Colloid Interface Sci. 273, 102034.

Sazhin, S., 2014. Droplets and Sprays. Springer, London.

Segredo-Otero, E., Sanjuán, R., 2020. The role of spatial structure in the evolution of viral innate immunity evasion: A diffusion-reaction cellular automaton model. PLoS Comput. Biol. 16, e1007656.

Stadnytskyi, V., Bax, C.E., Bax, A., Anfinrud, P., 2020. The airborne lifetime of small speech droplets and their potential importance in SARS-CoV-2 transmission. Proc. Natl. Acad. Sci. USA 117, 11875–11877.

Sze To, G.N., Wan, M.P., Chao, C.Y.H., Fang, L., Melikov, A., 2009. Experimental study of dispersion and deposition of expiratory aerosols in aircraft cabins and impact on infectious disease transmission. Aerosol Sci. Technol. 43, 466–485.

Tkachenko, A.V., Maslov, S., Elbanna, A., Wong, G.N., Weiner, Z.J., Goldenfeld, N., 2020. Persistent heterogeneity not short-term overdispersion determines herd immunity to COVID-19. http://dx.doi.org/10.1101/2020.07.26.20162420, medRxiv preprint.

Vejerano, E.P., Marr, L.C., 2018. Physico-chemical characteristics of evaporating respiratory fluid droplets. J. R. Soc. Interface 15, 20170939.

Verma, S., Dhanak, M., Frankenfield, J., 2020. Visualizing the effectiveness of face masks in obstructing respiratory jets. Phys. Fluids 32, 061708.

Wang, B., Wu, H., Wan, X.-F., 2020a. Transport and fate of human expiratory droplets - a modeling approach. Phys. Fluids 32, 083307.

Wang, B., Wu, H., Wan, X.-F., 2020b. Virus transmission from urinals. Phys. Fluids 32, 081703.

Whitman, J., Dhanji, A., Hayot, F., Sealfon, S.C., Jayaprakash, C., 2020. Spatio-temporal dynamics of host-virus competition: A model study of influenza A. J. Theoret. Biol. 484, 110026.

Wölfel, R., et al., 2020. Virological assessment of hospitalized patients with COVID-2019. Nature 581, 465–469.

Wu, F., et al., 2020. A new coronavirus associated with human respiratory disease in China. Nature 579, 265–269.

Xie, X., Li, Y., Chwang, A.T.Y., Ho, P.L., Seto, W.H., 2007. How far droplets can move in indoor environments – revisiting the Wells evaporation-falling curve. Indoor Air 17, 211–225.

Xu, F., Laguna, L., Sarkar, A., 2019. Aging-related changes in quantity and quality of saliva: Where do we stand in our understanding? J. Texture Stud. 50, 27–35.

Yang, X., et al., 2020. Transmission of pathogen-laden expiratory droplets in a coach bus. J. Hazard. Mater. 397, 122609.

Yezli, S., Otter, J.A., 2011. Minimum infective dose of the major human respiratory and enteric viruses transmitted through food and the environment. Food Environ. Virol. 3, 1–30.

Yin, J., Redovich, J., 2018. Kinetic modeling of virus growth in cells. Microbiol. Mol. Biol. Rev. 82, e00066-17.

Zhang, Y., Feng, G., Bi, Y., Cai, Y., Zhang, Z., Cao, G., 2019. Distribution of droplet aerosols generated by mouth coughing and nose breathing in an air-conditioned room. Sustain. Cities Soc. 51, 101721.

Zhang, Y., Kutateladze, T.G., 2020. Molecular structure analyses suggest strategies to therapeutically target SARS-CoV-2. Nat. Commun. 11, 2920.

Zhang, H., Li, D., Xie, L., Xiao, Y., 2015. Documentary research of human respiratory droplet characteristics. Proc. Eng. 121, 1365–1374.

Zhdanov, V.P., 1991. Elementary Physicochemical Processes on Solid Surfaces. Plenum, New York, Sec. 7.

Zhdanov, V.P., 2005. Monte Carlo simulation of bifurcation in the intracellular viral kinetics. Phys. Biol. 2, 46–50.

Zhdanov, V.P., 2011. Kinetic models of gene expression including non-coding RNAs. Phys. Rep. 500, 1–42.

Zhdanov, V.P., 2015. Kinetics of virus entry by endocytosis. Phys. Rev. E 91, 042715.

Zhdanov, V.P., 2018. Initial phase of replication of plus-stranded RNA viruses. Biophys. Rev. Lett. 13, 93–108.

Zhdanov, V.P., 2019. Slow relaxation during and after perturbation of bistable kinetics of gene expression. Eur. Biophys. J. 48, 297–302.

Zhu, N., et al., 2020. A novel coronavirus from patients with pneumonia in China, 2019. New Engl. J. Med. 382, 727–733.

Zwart, M.P., Daros, J.-A., Elena, S.F., 2011. One is enough: *in vivo* effective population size is dose-dependent for a plant RNA virus. PLoS Pathog. 7, e1002122.

Zwart, M.P., Elena, S.F., 2015. Matters of size: Genetic bottlenecks in virus infection and their potential impact on evolution. Annu. Rev. Virol. 2, 161–179.

Zwart, M.P., et al., 2009. An experimental test of the independent action hypothesis in virus-insect pathosystems. Proc. R. Soc. B 276, 2233–2242.